ELSEVIER

Chemical Engineering Journal 139 (2008) 136–146

Chemical Engineering Journal

www.elsevier.com/locate/cej

Simulation of effect of catalytic particle clustering on methane steam reforming in a circulating fluidized bed reformer

Wang Shuyan [a], Yin Lijie [a], Lu Huilin [a,*], He Yurong [a], Jianmian Ding [b], Liu Guodong [a], Li Xiang [a]

[a] *School of Energy Science and Engineering, Harbin Institute of Technology, Harbin 150001, China*
[b] *MSC Software, 2 MacArthur Place, Santa Ana, CA 92707, USA*

Received 9 April 2007; received in revised form 26 July 2007; accepted 27 July 2007

Abstract

Effect of catalytic particle clustering on methane steam reforming in a circulating fluidized bed (CFB) reformer is analyzed numerically using a two-dimensional hydrodynamic model coupling with methane steam reforming reaction kinetics. Gas flow fields and distributions of temperature and gas species in a Haldor Topsoe Ni/Mg Al_2O_4 spinel catalytic particle cluster are predicted. The computed results indicate that the rates of methane steam reaction of a catalyst particle in the cluster are less than that of an isolated catalyst particle out side the cluster. The yields of H_2, CO and H_2O in the cluster increase with the increase of operating temperature and inlet gas velocity but decrease with the increase of reactor pressure and feed steam.

Keywords: Methane steam reforming; Catalyst particle cluster; Circulating fluidized bed reformer; Numerical simulations

1. Introduction

Steam reforming of light hydrocarbons is an industrially important chemical reaction and a key step for producing hydrogen and syngas [1,2]. About 50% of hydrogen comes from methane steam reforming [3,4]. Recent demanding for hydrogen that utilized by many processes such as oil refining, methanol, metallurgy, ammonia, etc., have imposed a strong economic incentive to improve the hydrogen production technology.

The methane steam reforming are endothermic reactions favored at high temperature. The conventional steam reformers are fixed-bed catalytic reactors with catalyst loaded in a number of tubes placed in a furnace. The conventional fixed-bed reformers have some disadvantages such as low heat transfer rates, diffusion resistance in the catalyst pores, and large temperature gradients [5–9]. The endothermic reforming reaction processes are inefficient because of less heat transferred into the reformer. Moreover, the reactions produce significant quantities of carbon dioxide. The fluidized bed reformer is an attractive option in the syngas production because of high rate of heat transfer to maintain the isothermal operation. The overall process is generally integrated with the fluidized-bed combustor and reformer [10–14] to obtain advantages of thermodynamic equilibrium, more methane conversion and high hydrogen yield. In order to improve further the performance of methane reforming and catalyst regeneration, the circulating fluidized bed (CFB) has been widely utilized [15–18] as chemical processing unit. The CFB reformer can also be a major unit for hydrogen production. In a CFB reformer, the deactivated catalyst flowing out of the reformer with the exit gas stream can be separated in a gas–solid separator [19]. The regenerated catalyst is can then be recycled to the CFB riser. The carbon is completely burned in an integrated combustor and the catalyst is fully regenerated in the overall process. The fluidized solid catalyst particles acted as an internal heat carrier provide uniform reacting temperature in the riser. More steam may be provided to the reformer to avoid formation of coke and to achieve the high hydrogen yield.

It is generally agreed that the suspended particles may partly form clusters moving upward in the center, and downward near the riser walls in the risers [20]. Experiments have demonstrated the flow behavior of clusters in circulating fluidized beds and obtained the cluster motion, cluster formation time, time-

* Corresponding author. Tel.: +86 10 451 8641 2258; fax: +86 10 451 8622 1048.
E-mail address: huilin@hit.edu.cn (L. Huilin).

1385-8947/$ – see front matter © 2007 Elsevier B.V. All rights reserved.
doi:10.1016/j.cej.2007.07.097

Nomenclature

C_g	gas specific heat (kJ/(m^3 K))
C_1, C_2	empirically determined constants
d_p	particle diameter (m)
D	molecular diffusion coefficient (m^2/s)
D_c	diameter of cluster (m)
D_{CH_4}	diffusion coefficient of CH_4 (m^2/s)
g	gravity (m/s^2)
G_k	turbulent kinetic energy production (kg/(m s^3))
G_R	production due to reaction (kg/(m s^3))
h	convective heat transfer coefficient (kJ/(m^2 s K))
ΔH_j	heat of reaction for reaction j (kJ/kmol)
i, j, k	coordinate direction
k	turbulent kinetic energy (m^2/s^2)
k_1	rate constant for (A) (mol Pa$^{0.5}$/(kg s))
k_2	rate constant for (B) (mol/(Pa kg s))
K_{CO_2}	adsorption equilibrium constant of CO_2 (Pa^{-1})
K_{CO}	adsorption equilibrium constant of CO (Pa^{-1})
K_{CH_4}	adsorption equilibrium constant of CH_4 (Pa^{-1})
K_{H_2O}	adsorption equilibrium constant of H_2O (Pa^{-1})
K_1	equilibrium constant (Pa^2)
K_2	equilibrium constant, dimensionless
M_i	molecular weight of species i (kg/kmol)
n	particle number
p	gas pressure (Pa)
P_i	partial pressure of component i (Pa)
r	radial direction (m)
r_i	rate of reaction i (kmol/(kg s))
R	radius of particle (m)
R_c	radius of cluster (m)
T	temperature (K)
u_g	inlet gas velocity (m/s)
u_m	mean axial velocity of gas (m/s)
x	vertical coordinate (m)
Y_i	mass fraction of species i

Greek symbols

ε	energy dissipation rate (m^2/s^3)
ε_g	porosity
λ_g	thermal conductivity of gas (kJ/(m s K))
μ_g	gas viscosity (kg/(m s))
μ_l	laminar gas viscosity (kg/(m s))
ν_t	kinematic viscosity (m^2/s)
ρ_c	catalytic density (kg/m^3)
ρ_g	gas density (kg/m^3)
σ	empirically determined constant
ϕ_j	catalyst activity function

Subscripts

A, B, C	reaction routes
g	gas phase
R	at particle surface
s	solid phase

fraction of existence and occurrence in CFB risers [21–27]. Hence, in-depth knowledge about particle clustering effect on reactions in CFB riser is useful in predicting performance of circulating fluidized bed reactors and hence the design the CFB reactor.

In this work, we numerically investigate the effect of catalyst particle clustering on methane steam reforming with a Ni/Al_2O_3 catalyst particle cluster using a simplified two-dimensional hydrodynamic model with catalytic chemical reactions. Gas flow fields and distributions of gas temperature and gas species in the cluster are predicted. The effects of gas temperature, inlet gas velocity and reactor pressure on methane reforming are presented.

2. Mathematical models

Fig. 1 shows the geometry of the cluster. A cluster is modeled as a round two-dimensional disk in the riser. The radius of the cluster disk is R_c. Each particle in the cluster was labeled. Particles in the cluster are uniformly arranged in the cluster, and remain stationary. Particle diameter and density are assumed to be constant during reforming reactions. Radiation heat transfer between gas and particle is much small compared with convective heat transfer, and therefore, neglected. Radiation heat transfer between particles and the walls, and heat transfer between gas and catalyst particle are not considered in present study. The conservation equations of mass, species and energy in Eulerian coordinates are given as follows.

2.1. Gas phase continuity equation

The mass conservation equation of gas can be written as follows [28,29]:

$$\frac{\partial \rho_g}{\partial t} + \frac{\partial}{\partial x_j}(\rho_g u_j) = 0 \quad (1)$$

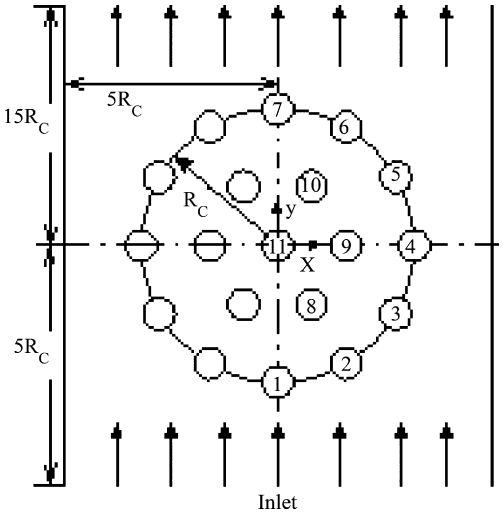

Fig. 1. Scheme of catalyst particle cluster.

2.2. Gas phase momentum equation

The conservation of momentum for gas phase is expressed as follows [28,29]:

$$\frac{\partial}{\partial t}(\rho_g u_i) + \frac{\partial}{\partial x_j}(\rho_g u_j u_i) = \frac{\partial p}{\partial x_i} + \frac{\partial}{\partial x_j}\left(\mu_g \frac{\partial u_j}{\partial x_i}\right) + \frac{\partial}{\partial x_j}\left(\mu_g \frac{\partial u_i}{\partial x_j}\right) + \rho_g g \quad (2)$$

where $\mu_g = \mu_l + \mu_t$ is the effective viscosity and $\mu_t = C_\mu \rho_g k^2/\varepsilon$ is the gas phase turbulent viscosity, which was modeled by k-ε turbulent model given below.

2.3. Turbulence model for gas phase

In present study, we employ the standard k-ε turbulence model for simulating turbulent flow in the riser. The standard k-ε turbulence model gives gas phase equations of turbulent kinetic energy [29]

$$\frac{\partial}{\partial t}(\rho_g k) + \frac{\partial}{\partial x_j}(\rho_g u_j k) = \frac{\partial}{\partial x_j}\left(\frac{\mu_t}{\sigma_k}\frac{\partial k}{\partial x_j}\right) + G_k - \rho_g \varepsilon \quad (3)$$

and turbulent kinetic energy dissipation rate

$$\frac{\partial}{\partial t}(\rho_g \varepsilon) + \frac{\partial}{\partial x_j}(\rho_g u_j \varepsilon) = \frac{\partial}{\partial x_j}\left(\frac{\mu_t}{\sigma_\varepsilon}\frac{\partial \varepsilon}{\partial x_j}\right) + \frac{\varepsilon}{k}[C_1 G_k - C_2 \rho_g \varepsilon] \quad (4)$$

where G_k is the production term,

$$G_k = \mu_g\left(\frac{\partial u_i}{\partial x_j} + \frac{\partial u_j}{\partial x_i}\right)\frac{\partial u_i}{\partial x_j} - \frac{2}{3}\delta_{ij}\frac{\partial u_k}{\partial x_k} \quad (5)$$

The empirical constants, C_μ, σ_ε, C_1 and C_2, are listed in Table 1.

2.4. Energy conservation of gas phase

The energy balance equation of gas phase is written as follows [28,29]:

$$\frac{\partial}{\partial t}(C_g T_g) + \frac{\partial}{\partial x_j}(u_j C_g T_g) = \frac{\partial}{\partial x_j}\left[\left(\lambda_g + \frac{C_g \nu_t}{\sigma_h}\right)\frac{\partial T_g}{\partial x_j}\right] + \sum_i \rho_c \Delta H_i r_i \quad (6)$$

where r_i is the reaction rates of routes A, B and C. As in previous assumption, radiation heat transfer process is not included in Eq. (6).

2.5. Species conservation equation of gas phase

The mass balance for a gas species k ($k = CO_2$, CO, H_2O and CH_4) is [28]

$$\frac{\partial}{\partial t}(\rho_g Y_k) + \frac{\partial}{\partial x_j}(\rho_g u_j Y_k) = \frac{\partial}{\partial x_j}\left[\left(\rho_k D_k + \frac{\mu_t}{\sigma_Y}\right)\frac{\partial Y_k}{\partial x_j}\right] + \sum_i \rho_c M_i r_{i,k} \quad (7)$$

where Y_k is the local mass fraction of species k, D_k the molecular diffusion coefficient, σ_Y is the turbulent Schmidt number ($\sigma_Y = 0.7$). The last term at right hand side of Eq. (7) is mass source from methane reforming reactions.

2.6. Reaction kinetics

Methane steam reforming reaction models associated with the different rate expressions were proposed [30–34]. Abashar investigated the mathematical models coupling with methane reforming with Haldor Topsoe Ni/Mg Al_2O_4 spinel catalyst particles in fluidized bed [4]. Based on the work of Xu and Froment [30], the following reaction rates consisting of three representative reactions are used for methane steam reforming and water-shift reactions with Haldor Topsoe Ni/Mg Al_2O_4 spinel catalyst particles:

$$CH_4 + H_2O \leftrightarrow CO + 3H_2 \qquad \Delta H_{298} = 206.0\,\text{kJ/mol} \quad \text{(A)}$$

$$r_1 = k_1 \frac{(P_{CH_4} P_{H_2O}/P_{H_2}^{2.5}) - (P_{CO} P_{H_2}^{0.5}/K_1)}{\text{DEN}^2} \quad (8)$$

Table 1
Parameters used in the simulations

Inlet gas velocity	1.0 m/s	Diameter of particle	100 μm
Total pressure	0.1 MPa	Diameter of cluster	975 μm
Inlet gas temperature	750 K	Number of particles	19
Inlet mass fraction of CH_4	0.2286	Temperature of particle	750 K
Inlet mass fraction of H_2O	0.7714	Particle density	3900 kg/m^3
Gas density	0.2847 kg/m^3	Porosity of cluster	0.8
Gas viscosity	1.546×10^{-5} kg/m-s	Empirically determined constant C_1	1.44
Diffusion coefficient of CH_4	2.064×10^{-5} m^2/s	Empirically determined constant C_μ	0.09
Diffusion coefficient of H_2O	2.178×10^{-5} m^2/s	Empirically determined constant σ_ε	1.3
Diffusion coefficient of CO_2	1.381×10^{-5} m^2/s	Empirically determined constant C_2	1.92
Diffusion coefficient of CO	1.92×10^{-5} m^2/s	Empirically determined constant σ_k	1.0
Diffusion coefficient of H_2	6.34×10^{-5} m^2/s	Empirically determined constant σ_h	1.0

$$CO + H_2O \leftrightarrow CO_2 + H_2 \qquad \Delta H_{298} = -41.0\,\text{kJ/mol} \quad \text{(B)}$$

$$r_2 = k_2 \frac{(P_{CO} P_{H_2O}/P_{H_2}) - (P_{CO_2}/K_2)}{\text{DEN}^2} \tag{9}$$

$$CH_4 + 2H_2O \leftrightarrow CO_2 + 4H_2 \qquad \Delta H_{298} = 164.9\,\text{kJ/mol} \quad \text{(C)}$$

$$r_3 = k_3 \frac{(P_{CH_4} P_{H_2O}^2/P_{H_2}^{3.5}) - (P_{CO_2} P_{H_2}^{0.5}/K_1 K_2)}{\text{DEN}^2} \tag{10}$$

$$\text{DEN} = 1 + K_{CH_4} P_{CH_4} + K_{H_2} P_{H_2} + K_{CO} P_{CO} + K_{H_2O} P_{H_2O}/P_{H_2} \tag{11}$$

where the reaction rate constants of reaction (A), (B) and (C) are, respectively

$$k_1 = 8.336 \times 10^{17} \exp\left(\frac{-28879.0}{T_g}\right) \quad (\text{mol Pa}^{0.5}/\text{kg s}) \tag{12}$$

$$k_2 = 12.19 \exp\left(\frac{-8074.3}{T_g}\right) \quad (\text{mol Pa}^{-1.0}/\text{kg s}) \tag{13}$$

$$k_3 = 2.012 \times 10^{17} \exp\left(\frac{-29336.0}{T_g}\right) \quad (\text{mol Pa}^{0.5}/\text{kg s}) \tag{14}$$

$$K_1 = 10266.76 \times 10^6 \exp\left(-26830.0/T_g + 30.11\right) \quad (\text{Pa}^2) \tag{15}$$

$$K_2 = \exp\left(4400.0/T_g - 4.063\right) \tag{16}$$

$$K_{CH_4} = 6.65 \times 10^{-9} \exp\left(\frac{4604.28}{T_g}\right) \quad (\text{Pa}^{-1}) \tag{17}$$

$$K_{H_2} = 6.12 \times 10^{-14} \left(\frac{9971.13}{T_g}\right) \quad (\text{Pa}^{-1}) \tag{18}$$

$$K_{CO} = 8.23 \times 10^{-10} \exp\left(\frac{8497.71}{T_g}\right) \quad (\text{Pa}^{-1}) \tag{19}$$

$$K_{H_2O} = 1.77 \times 10^5 \exp\left(\frac{-10666.35}{T_g}\right) \tag{20}$$

Carbon may be generated by the decompositions of hydrocarbons and carbon monoxide over reforming catalyst particles. The reaction rate will be affected by coke formation. The catalyst activity is defined as the ratio of the catalytic reaction rate to the initial reaction rate with fresh catalyst. Thus, the reaction rate r_j [34] for the deactivation of the catalyst can be expressed as

$$r_{c,j} = \phi_j r_j \tag{21}$$

where ϕ_j is catalyst activity function. In present simulations, the value of catalyst activity function is taken to be 1.0 and no carbon deposition is assumed.

2.7. Boundary conditions and simulation procedures

The inlet gas compositions, temperature and velocity were specified. At the outlet, the continuous gas and heat flow boundary conditions were used. No-slip boundary condition for gas flow at the particle surface is applied

$$u = k = \varepsilon = 0 \tag{22}$$

The boundary condition for gas species at the particle surface is

$$(\rho_k D_k + \frac{\mu_t}{\sigma_Y}) \frac{\partial Y_k}{\partial x_j}\bigg|_{R_c} = \sum \rho_c M_k r_k \tag{23}$$

The boundary condition of temperature at both particle and wall surfaces is

$$\frac{\partial T_g}{\partial x_j}\bigg|_{R_c} = 0 \tag{24}$$

The above equations are solved using the finite volume method [35] with appropriate boundary conditions. The cluster porosity can be calculated from $\varepsilon_g = (D_c^2 - n d_p^2)/D_c^2$, where D_c and n are the diameter of cluster and number of particles in the cluster, respectively. The parameters for the porosity calculation are listed in Table 1. Nineteen catalyst particles form the cluster and give a cluster porosity of 0.8. The physical domain of cylindrical boundary of each particle was mapped onto a square domain in the computation domain using the body-fitted coordinate to make the rectangular grids for the boundary of particles [36]. Fresh gases flow into the cluster, and react on the surface of catalyst particles. Sensitivity of the computed results to grid size was tested by increasing the number of computational grids until the grid size has no significant effect on the results. The grid size effect on the computed H_2/CO with various grids is shown in Fig. 13. It is noticed that the difference between the results from medium grid sizes (162 × 328) and those from finer grid sizes (196 × 374) is minor, but from coarse grid sizes (122 × 260). To reduce the computation times, the medium grid sizes were used through out all present computations except otherwise stated. A fixed time step of 1×10^{-5} s is used. The simulation runs 0.8 s of actual flow times. Fig. 2 shows the instantaneous mass fluxes of H_2, CO and CO_2 gas species and gas temperature at

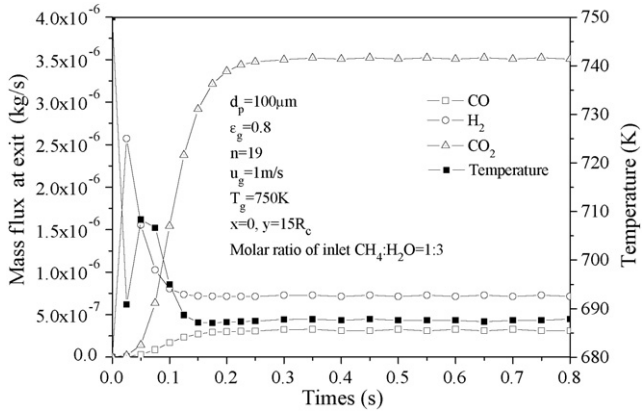

Fig. 2. Instantaneous mass flux of gases and temperature at exit.

the exit. Time-averaged values were calculated from last 0.5 s. A set of simulation needs about 24 h of CPU time on PC computer (80 GB hard disk, 128 Mb Ram and of 600 MHz CPU).

3. Simulation and analysis

3.1. Base case simulations

In the base simulations, the inlet gas velocity, inlet gas temperature, porosity and the reformer pressure were set to be 1.0 m/s, 750 K, 0.8 and 0.1 MPa, respectively, as listed in Table 1 except otherwise specified.

Fig. 3 shows the axial velocity of gas phase passing through the centerline of the cluster. The negative axial velocity means that gas backing flow in the down-stream, seeing Fig. 8a. The mean axial gas velocity through the cluster ($y = 0$), u_m, is calculated from computed axial velocities in the cluster domains. Ratio of mean axial velocity through the cluster to inlet gas velocity, u_m/u_g, is then determined. The results are shown in Fig. 4 [37]. Simulated results show that the ratio of gas velocity

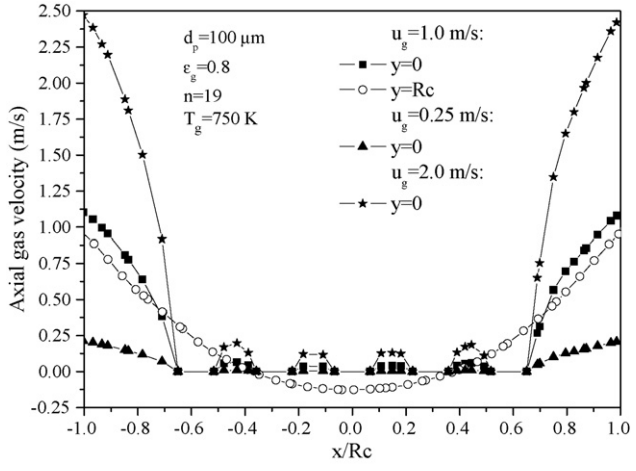

Fig. 3. Gas velocity distribution along lateral direction.

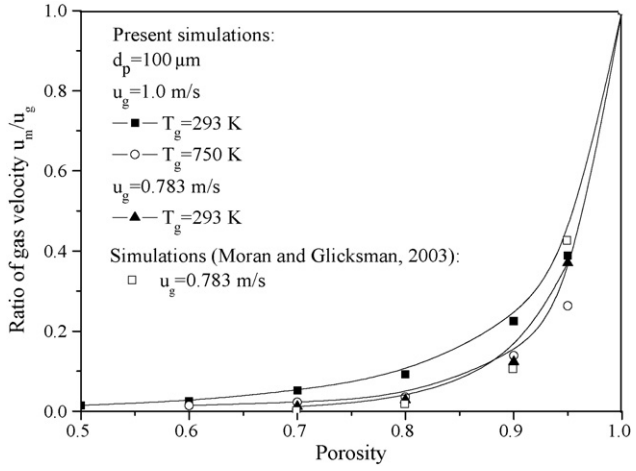

Fig. 4. Ratio of mean axial velocity through cluster to inlet gas velocity as a function of cluster porosity.

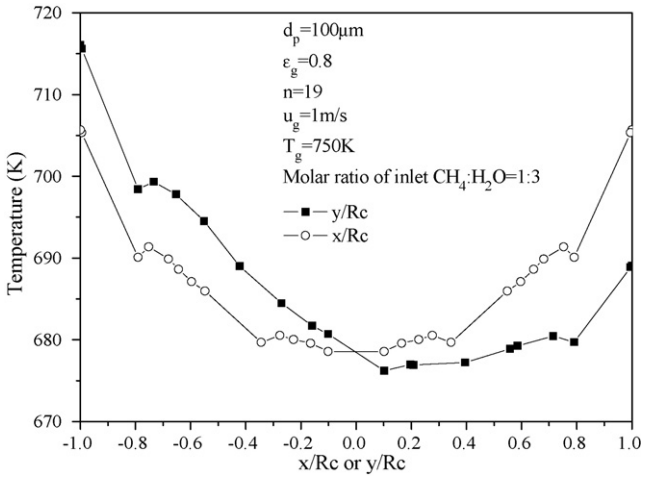

Fig. 5. Distributions of gas temperature along axial and lateral directions.

u_m/u_g is 0.035 for the base case. This means only about 3.5% of gases flow through the cluster, while most gas bypasses it due to the flow resistance of the cluster.

Fig. 5 shows the gas temperature distribution along axial and lateral directions of the cluster. The gas temperature decreases through the cluster due to endothermic reforming reaction. The high gas temperatures are located at the front of the cluster facing the incoming gas. The low gas temperature is at the backside of the cluster. In the radial direction, the gas temperature increases radially away from the cluster. The maximum of gas temperature difference in the cluster is about 40 K.

The variations of temperature and gas flux in the cluster can affect methane steam reforming of the cluster. Fig. 6 shows the reaction rates for some particles in the cluster and an insolated particle. Particles located in the front of the cluster have the high reaction rate r_1 and r_3, and low r_2 due to high gas temperature. We found that the reaction rate r_1 and r_3 of the isolated particle in the flowing stream was larger than that of particles in the cluster. Hence, particle clustering reduces the rates of methane steam reaction. Fig. 7 shows the axial and radial distributions of H_2, CO and CO_2 along the centerline of the cluster. In the

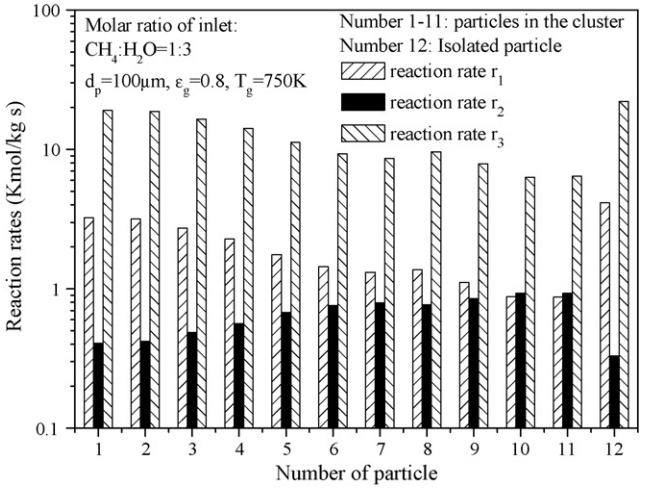

Fig. 6. Reaction rates of particle in the cluster.

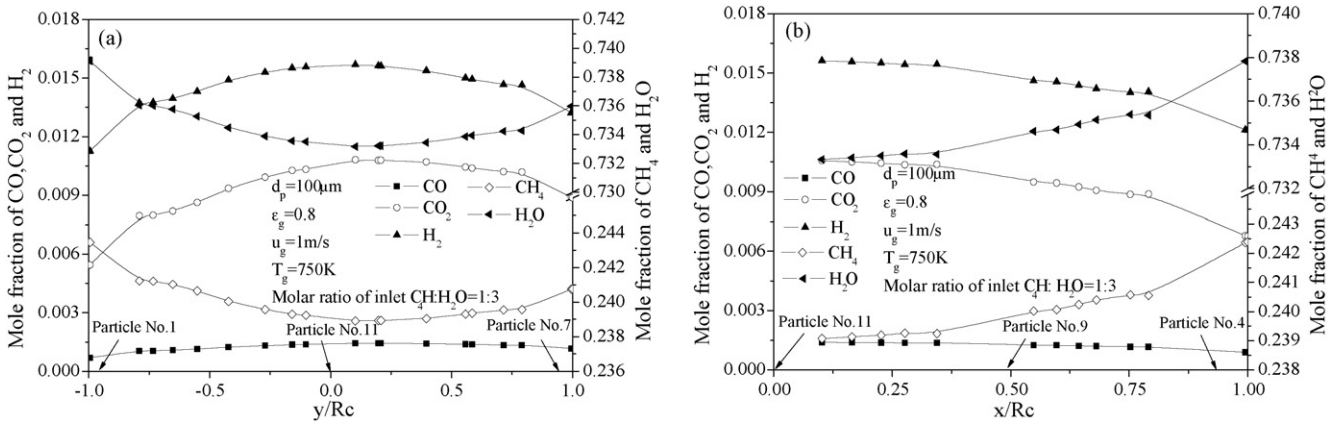

Fig. 7. Molar fractions of gas species along axial and lateral directions.

axial direction, the molar concentrations of H_2, CO and CO_2 species increase, reach a maximum at the cluster center, then decrease. The variation distributions of H_2O and CH_4 are caused by reforming reactions of (A) and (C). The high concentration of CO species at the tail of cluster is due to reforming shift reactions of (A) and (B). From the gases distribution in the lateral direction, we noticed that the non-uniformity of produced gases of CH_4 and H_2O in the cluster is affected by the uneven flow field in the cluster.

3.2. *Effect of cluster porosity*

The cluster porosity value can be changed by increase or decrease of the cluster size or number of particles occupied in the cluster. Fig. 8 shows the contour of gas axial velocity through the cluster at three different cluster porosities. With cluster diameters of 975, 1378 and 1949 μm, respectively, the corresponding cluster porosities are 0.8, 0.9 and 0.95, respectively. A vortex was formed at the back of the cluster at the cluster porosity of 0.8. With the increase of cluster porosity, the backing flow at the back of the cluster is disappeared. More gas can flow into the cluster with the increase of cluster porosity, and hence more methane is reformed in the cluster and the flow rates of H_2, CO and CO_2 species increased as well. Less CO and more H_2 selectivity are also observed.

The flow rate can be computed by summing the product of density and mass fraction of gas species and velocity with the dot product of the facet area vector and the facet velocity vector. Fig. 9a shows the flow rates of H_2, CO and CO_2 species as a function of cluster porosity. With the increase of porosity, more gas passes through the cluster. This will result in the increase of reaction rates. Hence with the increase of porosity less CO and more H_2 selectivity are observed. Fig. 9b shows the flow rate of CH_4 as a function of porosity. The molar ratio of H_2/CO was increased since more CH_4 are conversed into H_2 with the increase of porosity. Production of synthesis gas

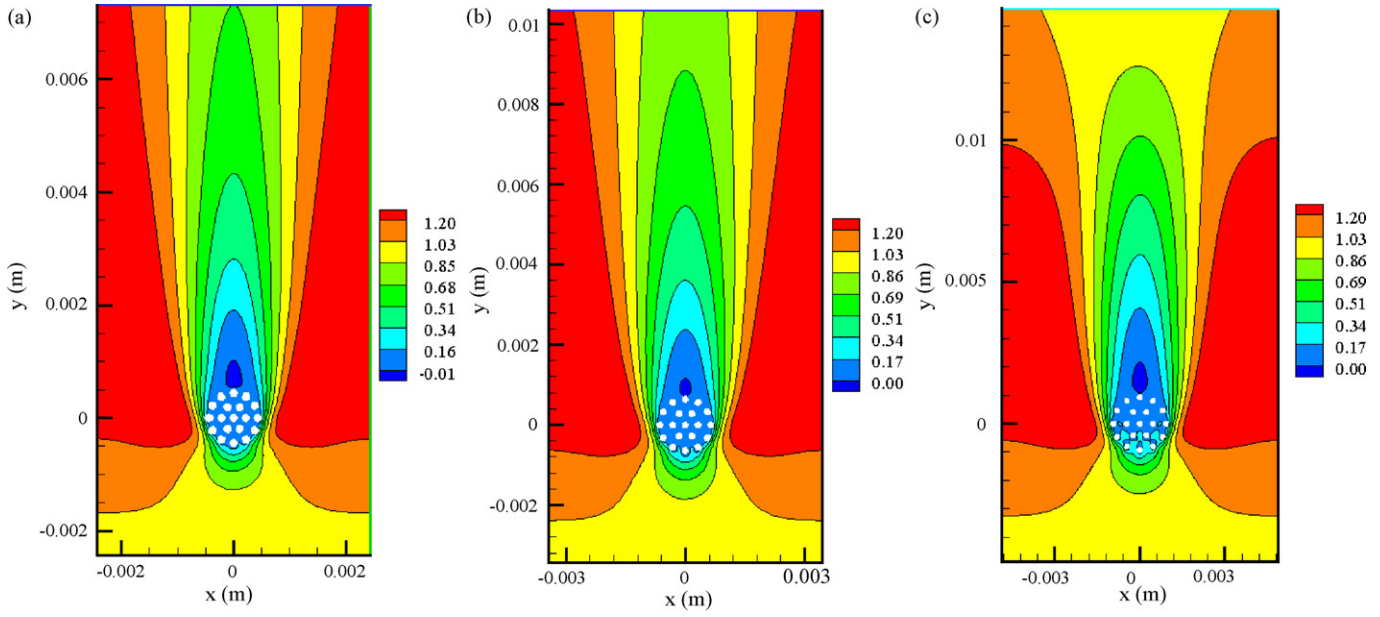

Fig. 8. Axial velocity of gas as a function of cluster porosities. (a) porosity = 0.8, (b) porosity = 0.9 and (c) porosity = 0.95.

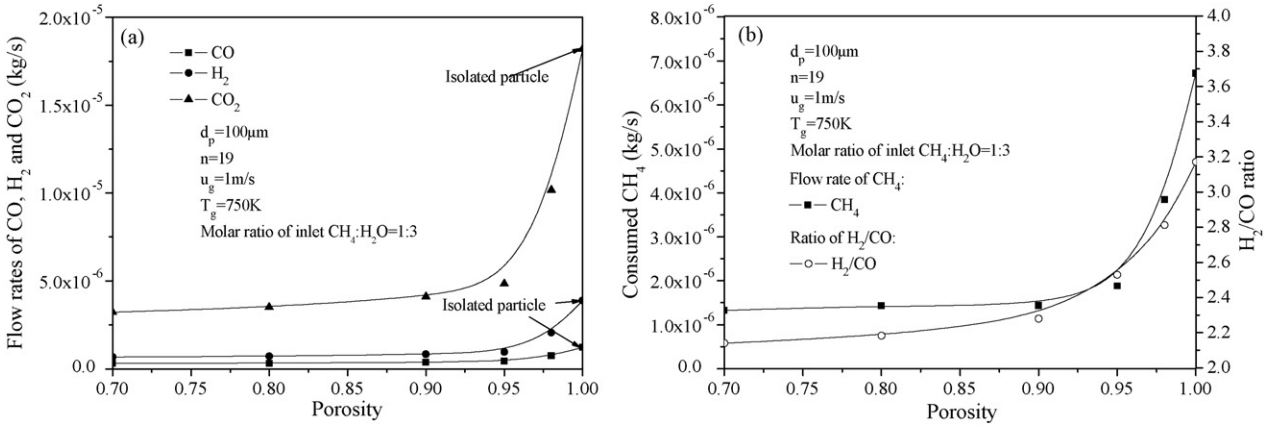

Fig. 9. Flow rates of gas species through the cluster as a function of porosity.

from methane and steam is influenced by the water-shift reaction (B). Steam reforming of methane is reduced due to the production of CO. Performance of methane steam reforming will be varied by the formation of the cluster. Computed results show that the produced gas species of an isolated particle is higher than any individual particle in the cluster. This indicates that the methane reforming was restrained by particle clustering in CFB reformers.

3.3. Effect of gas temperature

Increasing the operating temperature has a positive effect on the reforming reaction of methane since methane reforming is highly endothermic. Results of methane conversion and mass fraction of gases as a function of operating temperature are presented in Fig. 10a.

The effect of operating gas temperature on molar ratio of H_2/CO is shown in Fig. 10b. The molar ratio of H_2/CO decreases with the increase of operating temperature. The methane reforming reaction is dominant by the inlet gas temperature. On the other hand, the reverse reaction of water shifting is promoted at high temperature. From simulations, the decrease of H_2/CO ratios with increasing inlet gas temperature was observed. Therefore, the CFB can help to externally heat to raise the temperature of the reformer for achieving better reaction selectivity.

3.4. Effect of inlet gas velocity

With the increase of inlet gas velocity, more gases can flow through the cluster. Fig. 11a shows the flow rates of H_2, CO and CO_2 as a function of inlet gas velocities. The flow rates of gas species increase with the increase of inlet gas velocity as expected. More CH_4 is found in the cluster with more CH_4 introduced from the inlet. Yields of H_2, CO and CO_2 are altered with the inlet gas velocity.

The reformed methane flux as a function of inlet gas velocity by the cluster and the isolated particle are shown in Fig. 11b. With the increase of inlet gas velocity, the reformed methane by the cluster is monotonically increased but for an isolated particle the reformed methane flux increases to a point, and then decreases as the inlet gas velocity increases. This may be due to the more flow passing the particle if more flow is introduced the riser. Note that if the inlet gas velocity is high enough the cluster breakage may occur. However, the cluster breakage is not considered in present investigation.

The molar ratios of H_2/CO as a function of inlet gas velocity are shown in Fig. 11b. As the inlet gas velocity increases, the molar ratio is increased monotonously for both the cluster and the isolated particle.

Experiments and simulations have shown that the gas velocity is high in the riser center and low near the riser walls. With

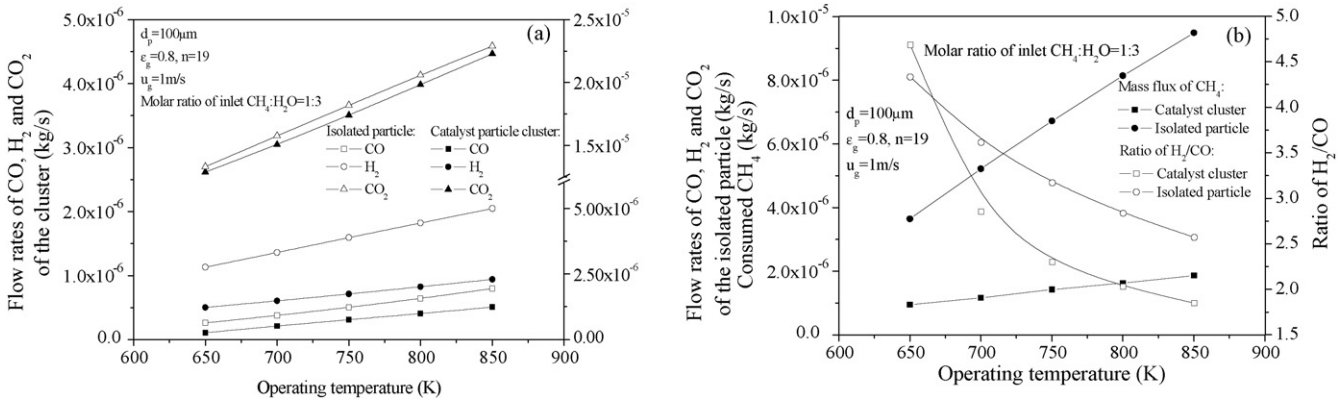

Fig. 10. Produced mass fluxes of gas species through the cluster as a function of operating temperature.

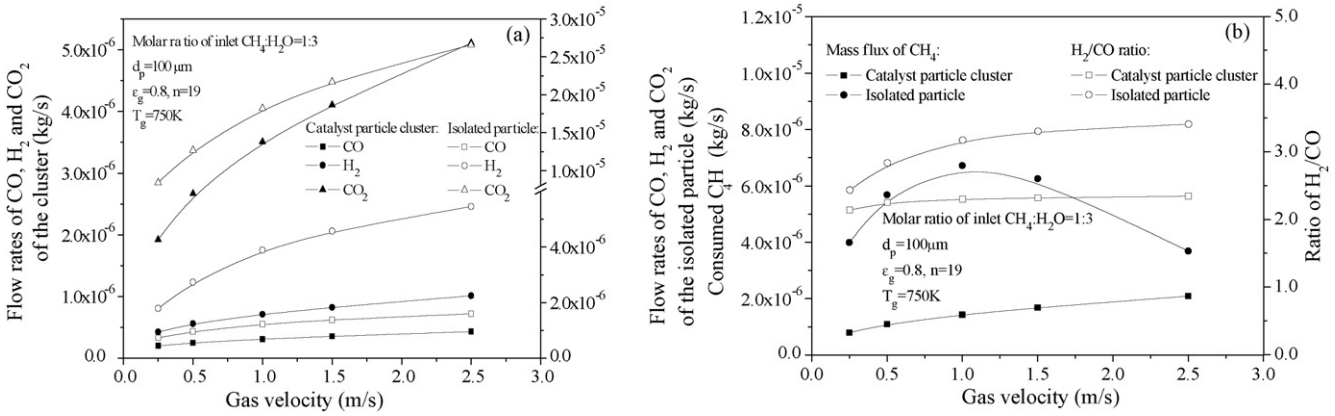

Fig. 11. Influence of inlet gas velocity on mass fluxes of gas species and ratio of H_2/CO.

uniform inlet gas velocity, the gas flow in the cluster located in the center of the riser is concavely distributed, as shown in Fig. 12. If the inlet gas velocity is linearly increased from the left to right of the riser and with same amount inlet flow rate, the shape of the flow distribution is still close to the case with uniform inlet velocity, but the H_2/CO ratio is slightly reduced for the case of non-uniform inlet gas velocity compared with the case of uniform inlet velocity, as shown in Fig. 13. Thus, the effect of inlet gas velocity distribution on methane steam reforming reaction of the cluster will not be important in the simulations.

3.5. *Effect of reactor pressure*

The rates of methane reforming reaction were related with reactor pressure. Fig. 14 shows the reaction rates r_1, r_2 and r_3 of the cluster as a function of reactor pressure. With the increase of reactor pressure, the reaction rates of reaction (A), (B) and (C) are decreased. Thus, the reaction will be rapidly decreased with the increase of reactor pressure.

The effect of reactor pressure on the concentration distributions of H_2, CO and CO_2 are shown in Fig. 15a. The reactions are thermodynamically favored at low pressure according to Le

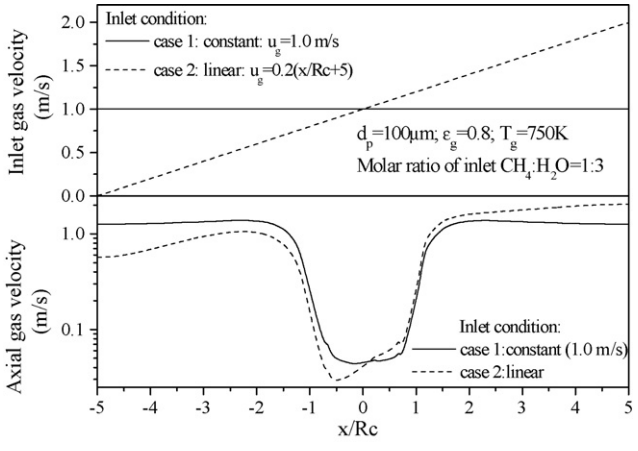

Fig. 12. Influence of inlet gas velocity boundary conditions on axial gas velocity through the centerline of cluster.

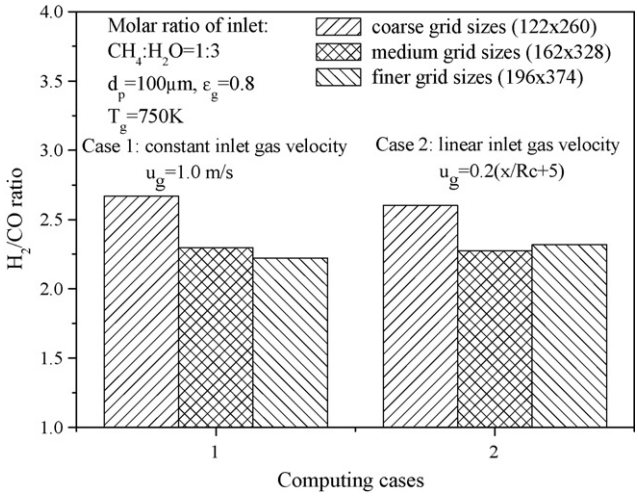

Fig. 13. Computed ratio of H_2/CO at two different inlet gas velocity boundary conditions.

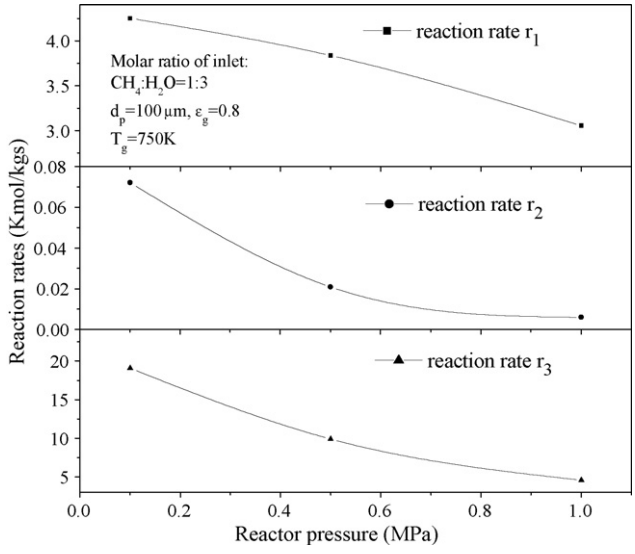

Fig. 14. Reaction rates of the cluster as a function of reactor pressure.

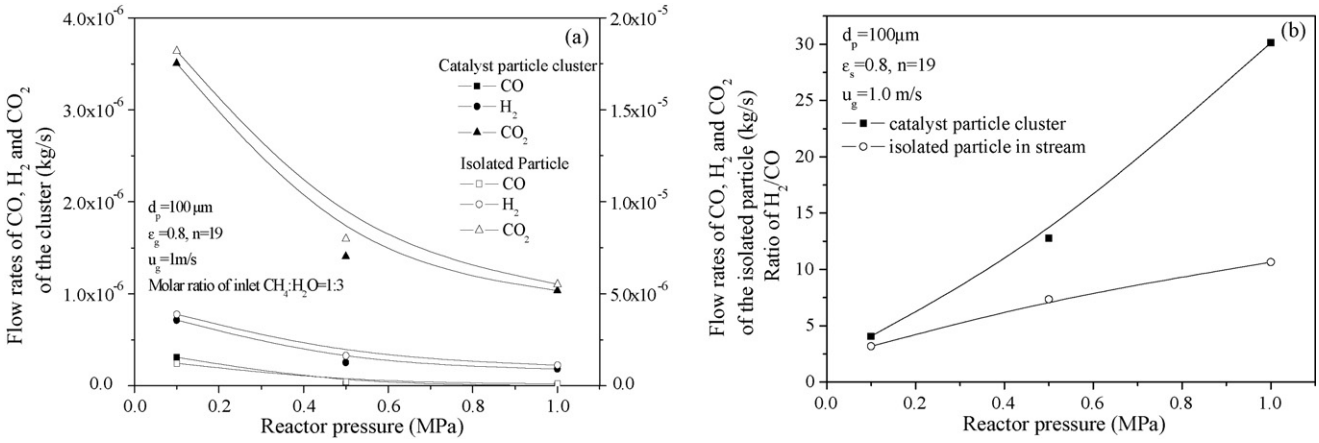

Fig. 15. Profiles of mass fluxes of gas species and molar ratio of H_2/CO as a function of reactor pressure.

Chatelier's principle [38]. Therefore, the flow rates of H_2, CO and CO_2 decrease with the increase of reactor pressure.

Effect of the reactor pressure on the molar ratio of H_2/CO is shown in Fig. 15b. It is shown that the ratios of H_2/CO increased with the increase of reactor pressure. The high pressure is thermodynamically unfavorable to the methane reforming.

3.6. Effect of H_2O/CH_4

Computed flow rates of gas species with various feed steam to methane ratios are shown in Fig. 16a. The same trends of gas species in the cluster and the isolated particle are observed. At a given temperature, the catalytic activity of Haldor Topsoe Ni/Mg Al_2O_4 spinal catalyst particles with respect to CH_4 mass fluxes decreased with the increase of the inlet steam to methane ratios from 2.0 to 4.0. In general, with more steam fed, more methane should be reformed. However, an optimum steam-feeding rate for the maximum methane conversion has to be evaluated since the steam generation is an expensive process.

As shown in Fig. 16b, the H_2/CO ratios increase with the steam to methane ratios from 2.0 to 4.0. Similarly, reforming with the cluster and the isolated particle alter the H_2/CO ratios. The steam may reduce the carbon deposition onto the catalyst particles [39]. The carbon deposited on the catalysts can be dramatically reduced with the addition of steam. Thus, steam plays an important role in the effective removal of carbon. However, as stated earlier, more steam will need more energy consumption. To produce hydrogen efficiently and economically, the steam to methane feed ratio has to keep in an economical value in industrial applications.

3.7. Effect of coke formation

Traditionally, methane steam reforming is carried out at high temperatures (around 800 °C), pressures between 1.6 and 4.1 MPa and steam to methane ratios within a range of 2–4. Deactivation of nickel catalysts by carbon formation is a significant issue in methane steam reforming caused by fouling of the Ni surface, blockage of the pores of the catalytic particle and disintegration of the support material [39]. Thermodynamically, the most probable reactions for carbon formation are the following equations [40–41]:

CH_4 cracking

$$CH_4 \leftrightarrow C + 2H_2 \qquad \Delta H_{298} = 122.3\,\text{kJ/mol} \tag{D}$$

Boudouard

$$2CO \leftrightarrow C + CO_2 \qquad \Delta H_{298} = -125.2\,\text{kJ/mol} \tag{E}$$

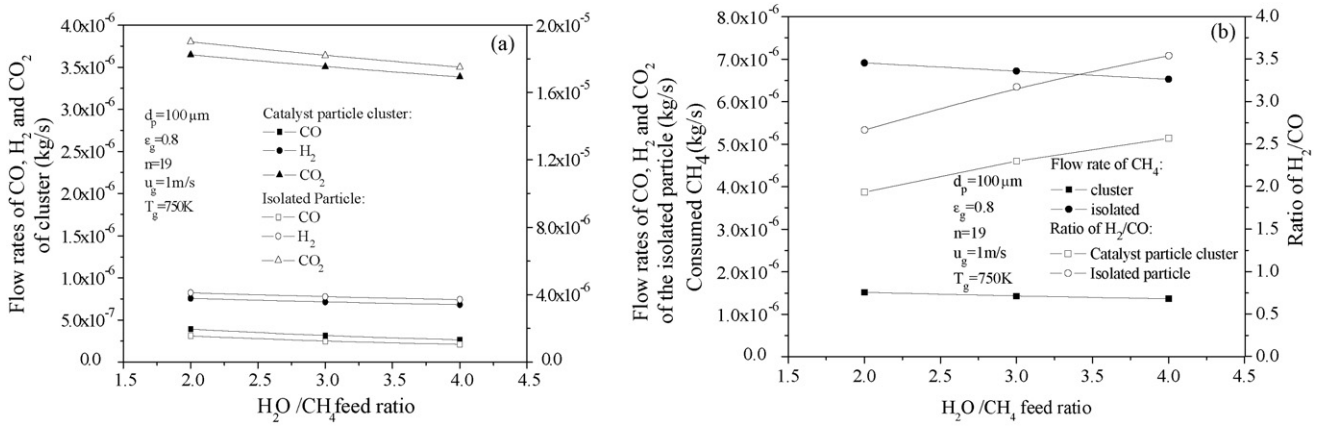

Fig. 16. Profiles of mass fluxes of gas species and molar ratio of H_2/CO at three different feed steam and methane ratios.

CO reduction

$$CO + H_2 \leftrightarrow C + H_2O \qquad \Delta H_{298} = -84.0\,kJ/mol \qquad (F)$$

The net rate of carbon deposition (reactions (D)–(F)) is evaluated by means of the following kinetic expressions reported by Snoeck et al. [42]:

$$r_{C,net} = \frac{r_{C,D} + r_{C,(E+F)}}{DEN_C^2} \qquad (25)$$

where

$$r_{C,D} = k_M K_{CH_4} \left(p_{CH_4} - \frac{p_{H_2}^2}{K_{M,av}} \right) \qquad (26)$$

$$r_{C,(E+F)} = k_O \left(K_{O,H_2O} p_{CO} \frac{K_1}{K_{M,av}} - \frac{1}{K_{O,H_2O}} \frac{p_{H_2O}}{P_{H_2}} \right) \qquad (27)$$

$$DEN_C = 1 + \left(K_{CH_4} p_{CH_4} + \frac{1}{K_r} p_{H_2}^{3/2} + \frac{1}{K_{O,H_2O}} \frac{p_{H_2O}}{P_{H_2}} \right) \qquad (28)$$

The term $r_{C,D}$ of Eq. (25) represents the carbon formation by CH_4 cracking and its gasification by H_2 (reaction (D)), while $r_{C,(E+F)}$ groups the carbon formation by reactions (E) and (F), and its gasification by CO_2 and H_2O. Applying the Arrhenius equation and van't Hoff equation to these parameters

$$k_M = 55619 \ \exp\left(-\frac{65053}{RT_g}\right),$$

$$k_O = 1.67 \times 10^9 \ \exp\left(-\frac{148916}{RT_g}\right) \qquad (29)$$

$$K_r = 251893 \ \exp\left(-\frac{95489}{RT_g}\right),$$

$$K_{O,H_2O} = 17372 \ \exp\left(-\frac{60615}{RT_g}\right),$$

$$K_{M,av} = 2.47 \times 10^7 \ \exp\left(-\frac{122325}{RT_g}\right) \qquad (30)$$

The values of these coefficients involved in Eqs. (26)–(29) can be found in [42]. The net rate of carbon formation has been assumed deposition on the surface of each particle in the cluster. Once the model is solved and the gas composition and temperature profiles are known, the $r_{c,net}$ expression is used to calculate the potential of carbon formation of each particle in the cluster. According to the kinetic criterion, if $r_{c,net} \geq 0$ at any position in the reactor, carbon deposition occurs [42].

Fig. 17 shows the H_2/CO ratios with and without the coke formation at the cluster porosity of 0.8. Compared to the case without the coke formation, the H_2/CO ratio is reduced with the coke formation. Since the reaction rates (A) and (C) are decreased with the coke formation. The consumed CH_4 reduced from 1.631×10^{-6} kg/s without the coke formation to 1.614×10^{-6} kg/s with the coke formation in the cluster. Due to the Boudouard and the CO reduction, the CO_2 concentration is increased and more carbon produced. Thus, the coke formation will reduce the H_2/CO ratio in the clusters.

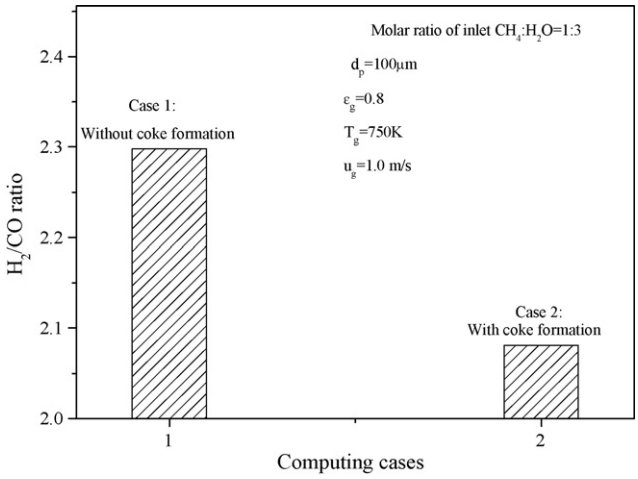

Fig. 17. Effect of coke formation on H_2/CO ratios.

4. Conclusions

A mathematical model for predicting methane steam reforming of Haldor Topsoe Ni/Mg Al_2O_4 spinel catalyst particles cluster is proposed by coupling hydrodynamics with catalytic methane steam reactions. Flow behavior of gases in the cluster was investigated. The distributions of gas temperature and mass fraction of gas species are predicted. The yields of H_2, CO and methane conversions increase with the increase of the cluster porosity, temperature and inlet gas velocity, but decrease with the increase of the steam to methane ratio and operating pressure.

The catalyst particle clustering strongly affects flow behavior and methane steam reforming in a CFB reformer. Present simulations provided a preliminary picture for the start of simulations of methane steam CFB reformers. To more accurately predict flow behavior on methane reforming, carbonation effect on reforming reactions should be considered. Detail models for cluster formation and deformation are also need to be developed. These models will be included in our future simulations for the CFB reformers.

Acknowledgement

This work was supported by Natural Science Foundation of China through grant nos. 50620120442 and 20606006 and NSFC-Petro China Company Limited under the cooperative project no. 20490200.

References

[1] J.N. Armor, Review: the multiple roles for catalysis in the production of H_2, Appl. Catal. A: Gen. 176 (1999) 159–176.

[2] A. Effendi, Z.G. Zhang, K. Hellgardt, K. Honda, T. Yoshida, Steam reforming of a clean model biogas over Ni/Al_2O_3 in fluidized- and fixed-bed reactors, Catal. Today 77 (2002) 181–189.

[3] G. Barbieri, D.M. Francesco, Simulation of the methane steam reforming process in a catalytic Pd-membrane reactor, Ind. Eng. Chem. Res. 36 (1997) 2121–2127.
[4] M.E.E. Abashar, Coupling of steam and dry reforming of methane in catalytic fluidized bed membrane reactors, Int. J. Hydrogen Energy 29 (2004) 799–808.
[5] J.R. Rostrup-Nielsen, Coking on nickel catalysts for steam reforming of hydrocarbons, J. Catal. 33 (1974) 184–201.
[6] A.M. Groote, G.F. Froment, Simulation of the catalytic partial oxidation of methane to synthesis gas, Appl. Catal. A: Gen. 138 (1996) 245–264.
[7] U. Olsbye, O. Moen, U.A. Slagtern, I.M. Dahl, An investigation of the coking properties of fixed and fluid bed reactors during methane-to-synthesis gas reactions, Appl. Catal. A: Gen. 228 (2002) 289–303.
[8] K. Tomishige, Syngas production from methane reforming with CO_2/H_2O and O_2 over NiO–MgO solid solution catalyst in fluidized bed reactors, Catal. Today 89 (2004) 405–418.
[9] K. Johnsen, H.J. Ryu, J.R. Grace, C.J. Lim, Sorption-enhanced steam reforming of methane in fluidized bed reactor with dolomite as CO_2-acceptor, Chem. Eng. Sci. 61 (2006) 1195–1202.
[10] A.M. Adris, C.J. Lim, J.R. Grace, The fluidized-bed membrane reactor for steam methane reforming: model verification and parametric study, Chem. Eng. Sci. 52 (1997) 1609–1622.
[11] S. Roy, B.B. Pruden, A.M. Adris, C.J. Lim, J.R. Grace, Fluidized-bed steam methane reforming with oxygen input, Chem. Eng. Sci. 54 (1999) 2095–2102.
[12] T. Wurzel, S. Malcus, L. Mleczko, Reaction engineering investigations of CO_2 reforming in a fluidized bed reactor, Chem. Eng. Sci. 55 (2000) 3955–3966.
[13] K. Tomishige, Y. Matsuo, Y. Sekine, K. Fujimoto, Effective methane reforming with CO_2 and O_2 under pressurized condition using NiO-MgO and fluidized bed reactor, Catal. Commun. 2 (2001) 11–15.
[14] M.A. Rakib, K.I. Alhumaizi, Modeling of a fluidized bed membrane reactor for the steam reforming of methane: Advantages of oxygen addition for favorable hydrogen production, Energy Fuels 19 (2005) 2129–2135.
[15] P. Prasad, S.S.E.H. Elnashaie, Novel circulating fluidized bed membrane reformer for the efficient production of ultraclean fuels from hydrocarbons, Ind. Eng. Chem. Res. 41 (2002) 6518–6527.
[16] Z. Chen, Y. Yan, S.S.E.H. Elnashaie, Novel circulating fast fluidized bed membrane reformer for efficient product ion of hydrogen from steam reforming of methane, Chem. Eng. Sci. 58 (2003) 4335–4349.
[17] J. Grace, A.E.M. Adris, T. Boyd, C.J. Lim, Hydrogen from an internally circulating fluidized bed membrane reactor, Int. J. Chem. Reactor Eng. 3 (2005) 1–12.
[18] S.S.E.H. Einashaie, P. Prasad, Z. Chen, Static bifurcation characteristics of an autothermal circulating fluidized bed hydrogen generator for fuel cells, Ind. Eng. Chem. Res. 44 (2005) 4871–4883.
[19] P. Prasad, S.S.E.H. Elnashaie, Coupled steam and oxidative reforming for hydrogen production in a novel membrane circulating fluidized-bed reformer, Ind. Eng. Chem. Res. 42 (2003) 4715–4722.
[20] K. Kunii, O. Levenspiel, Fluidization Engineering, second ed., Butterworth Heinemann, MA, USA, 1991.
[21] C.J. Chen, Experiments that address phenomenological issues in fast fluidization, Chem. Eng. Sci. 54 (1999) 5529–5539.
[22] A.K. Sharma, K. Tuzla, J. Matsen, J.C. Chen, Parametric effects of particle size and gas velocity on cluster characteristics in fast fluidized beds, Powder Technol. 111 (2000) 114–122.
[23] S.V. Manyele, J.H. Parssinen, J.X. Zhu, Characterizing particle aggregates in a high-density and high-flux CFB riser, Chem. Eng. J. 88 (2002) 151–161.
[24] M. Horio, H. Kuroki, Three-dimensional flow visualization of dilutely dispersed solids in bubbling and circulating fluidized beds, Chem. Eng. Sci. 49 (1994) 2413–2421.
[25] V.D. Moortel, E. Azario, R. Santini, L. Tadrist, Experimental analysis of the gas-particle flow in a circulating fluidized bed using a phase Doppler particle analyzer, Chem. Eng. Sci. 53 (1998) 1883–1899.
[26] P.D. Noymer, L.R. Glicksman, Cluster motion and particle-convective heat transfer at the wall of a circulating fluidized bed, Int. J. Heat Mass Transfer 41 (1998) 147–158.
[27] C. Guenther, R. Breault, Wavelet analysis to characterize cluster dynamics in a circulating fluidized bed, Powder Technol. 173 (2007) 163–173.
[28] G.F. Froment, K.B. Bischoff, Chemical Reactor Analysis and Design, second ed., Wiley, New York, 1990.
[29] V.V. Ranade, Computational Flow Modeling for Chemical Reactor Engineering, Plenum Press, New York, 2001.
[30] J. Xu, G.F. Froment, Methane steam reforming, methanation and water-gas shift: I. Intrinsic kinetics, AIChE J. 35 (1989) 88–96.
[31] S. Grevskott, T. Rusten, M. Hillestad, E. Edwin, O. Olsvik, Modelling and simulation of a steam reforming tube with furnace, Chem. Eng. Sci. 56 (2001) (2001) 597–603.
[32] K. Jarosch, T.E. Solh, H.I. de Lasa, Modelling the catalytic steam reforming of methane: discrimination between kinetic expressions using sequentially designed experiments, Chem. Eng. Sci. 57 (2002) 3439–3442.
[33] F. Gallucci, L. Paturzo, A. Basile, A simulation study of the steam reforming of methane in a dense tubular membrane reactor, Int. J. Hydrogen Energy 29 (2004) 611–617.
[34] Z. Chen, S.S.E.H. Elnashaie, Steady-state modeling and bifurcation behavior of circulating fluidized bed membrane reformer–regenerator for the production of hydrogen for fuel cells from heptane, Chem. Eng. Sci. 59 (2004) 3965–3979.
[35] S.V. Patankar, Numerical Heat Transfer and Fluid Flow, McGraw-Hill, New York, 1998.
[36] Z. Yunhau, L. Huilin, H. Yurong, J. Ding, Y. Lijie, Numerical prediction of combustion of carbon particle clusters in a circulating fluidized bed riser, Chem. Eng. J. 118 (2006) 1–10.
[37] J.C. Moran, L.R. Glicksman, Experimental and numerical studies on the gas flow surrounding a single cluster applied to a circulating fluidized bed, Chem. Eng. Sci. 58 (2003) 1879–1886.
[38] I.N. Levine, Physical Chemistry, McGraw-Hill, New York, 2002.
[39] D.L. Trimm, Coke formation and minimization during steam reforming reactions, Catal. Today 37 (1997) 233–238.
[40] J.R.R. Nielsen, Catalytic steam reforming, Catal. Sci. Technol. 1 (1984) 1–117.
[41] M.N. Pedernera, J. Pina, D.O. Borio, Kinetic evaluation of carbon formation in a membrane reactor for methane reforming, Chem. Eng. J. 134 (2007) 138–144.
[42] J.W. Snoeck, G.F. Froment, M. Fowles, Kinetic evaluation of carbon formation in steam/CO_2-natural gas reformers: influence of the catalyst activity and alkalinity, Int. J. Chem. Reactor Eng. A7 (2003) 1–16.